JACS
JOURNAL OF THE AMERICAN CHEMICAL SOCIETY

Article

pubs.acs.org/JACS

Terpyridine-Based, Flexible Tripods: From a Highly Symmetric Nanosphere to Temperature-Dependent, Irreversible, 3D Isomeric Macromolecular Nanocages

Sourav Chakraborty,[†,⊥] Wei Hong,[†,⊥] Kevin J. Endres,[†] Ting-Zheng Xie,[†] Lukasz Wojtas,[§] Charles N. Moorefield,[∥] Chrys Wesdemiotis,*[,†,‡] and George R. Newkome*[,†,‡]

[†]Department of Polymer Science and [‡]Department of Chemistry, The University of Akron, Akron, Ohio 44256, United States
[§]Department of Chemistry, University of South Florida, 4202 East Fowler Avenue, Tampa, Florida 33620, United States
[∥]Dendronex, LLC, 109 Runway Drive, Lubbock, Texas 79416, United States

Supporting Information

ABSTRACT: A three-dimensional, highly symmetric sphere-like nanocage was synthesized using a terpyridine (tpy)-based, flexible tris-dentate ligand and characterized by single crystal X-ray analysis. To introduce more rigidity, one of the tpy units of the tris-dentate ligand was preblocked by stable <tpy-Ru^{2+}-tpy> connectivity to form the corresponding Ru^{2+}-dimer. The complexation between Ru^{2+}-dimer and Fe^{2+} demonstrates an unexpected temperature-dependent assembly between two irreversible isomeric 3D nanocages. Investigation of the coordination process and structural configurations of the metal–ligand framework, affected by the introduction of rigidity and in the presence of external stimuli (temperature), is reported.

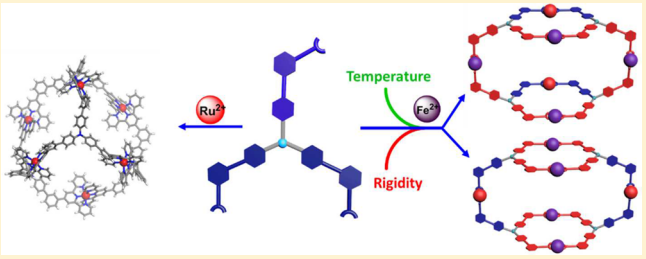

INTRODUCTION

Naturally occurring biological systems often utilize noncovalent supramolecular interactions to self-assemble into higher order architectures, such as the secondary and tertiary structures of proteins and DNA.[1,2] The positioning and directionality of these noncovalent interactions are essential for molecular recognition and formation of supramolecular assemblies.[3] Inspired by diverse systems, many efforts have been dedicated to the synthesis of complex metallosupramolecules, using metal-ligand coordination with its structural diversity. This can be realized by precise control over functional directionality of monomers with predefined bite angles.[4−24] Of the numerous examples, 2,2′:6′,2″-terpyridine (tpy) tectons have gained extensive attention due to their ability to coordinate diverse metals that facilitate both labile (Zn^{2+}, Cd^{2+}) and nonlabile (Ru^{2+}, Fe^{2+}, Os^{2+}) ligand-metal-ligand connectivity, thus permitting control over bond strength and ultimately the desired molecular architecture(s).[7,25−29] Use of linear coordinated pseudo-octahedral <tpy-M^{2+}-tpy> connectivity provides convenient synthetic characteristics to generate the edges of discrete 2D and 3D macromolecules with highly ordered organic vertices. Using tailored tpy-based monomers, we have reported the synthesis of several unique 2D metallomacrocycles (including triangles,[30] hexagons,[31] various spoked wheels,[32,33] a Sierpiński gasket[34] and triangle,[35] a molecular [4]-triangulane[36]) as well as a 3D nanosphere[37] and more recently precise molecular fusion and fission between cuboctahedron and octahedron motifs.[38,39] However, there are few 3D molecular cages, based on terpyridinyl ligands so far reported.[37−45] Considering the potential of terpyridine-based materials for biomedical applications[46,47] and optoelectronic devices,[47−50] the attraction to construct new 3D-terpyridinyl nanoarchitectures is compelling.

The formation of terpyridine-based nanostructures is a consequence of both kinetic and thermodynamic control; studies show that kinetically dominated complexation increases in the order Cd^{2+} < Zn^{2+} < Fe^{2+} < Os^{2+} < Ru^{2+}.[51] The latter forms stable coordinative bonds, in which thermodynamic control over the self-assembly process is essentially lost by the creation of an irreversible metal complex; whereas, the former provides more stable thermodynamic constructs. The interconversion between different thermodynamic and kinetic superstructures is only possible under appropriate external stimuli, such as concentration and temperature.[38,41,52] Although the use of nonlabile metals can be challenging for the construction of a discrete architecture involving multiple metal–ligand connectivity, potential advantages include a final product that is easy to isolate and purify. Relying on these advantages, a stepwise assembly procedure utilizing <tpy-Ru^{2+}-tpy> connectivity was used to design and construct several discrete architectures.[36,40,53]

Recently, we reported the construction of a highly symmetric nanosphere by combining a rigid tris-terpyridine monomer with

Received: November 14, 2016
Published: February 6, 2017

DOI: 10.1021/jacs.6b11784
J. Am. Chem. Soc. 2017, 139, 3012−3020

Scheme 1. Synthesis of Molecular Nanosphere 4 and Stepwise Assembly of Nanoarchitectures 6a, 6b, and 7

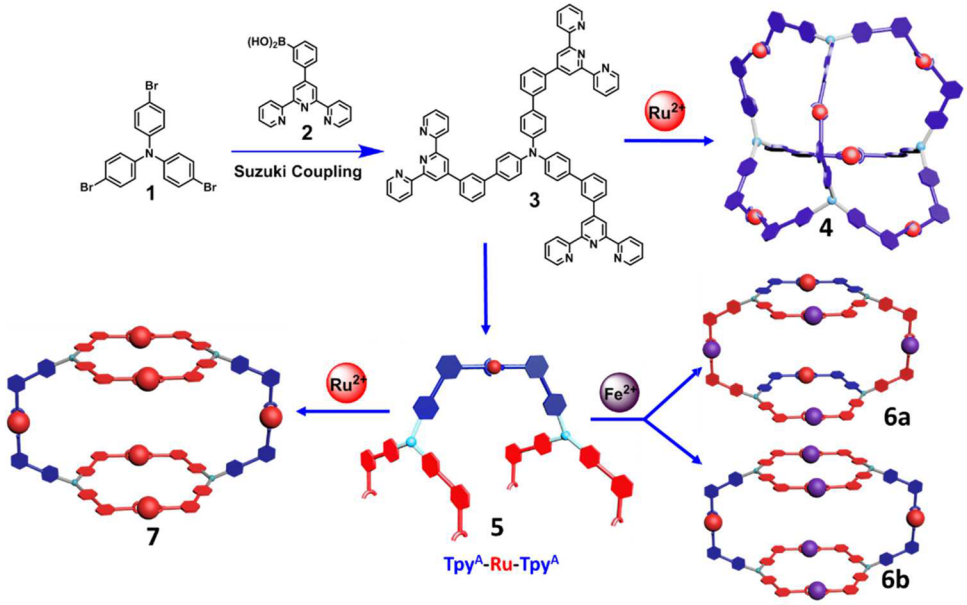

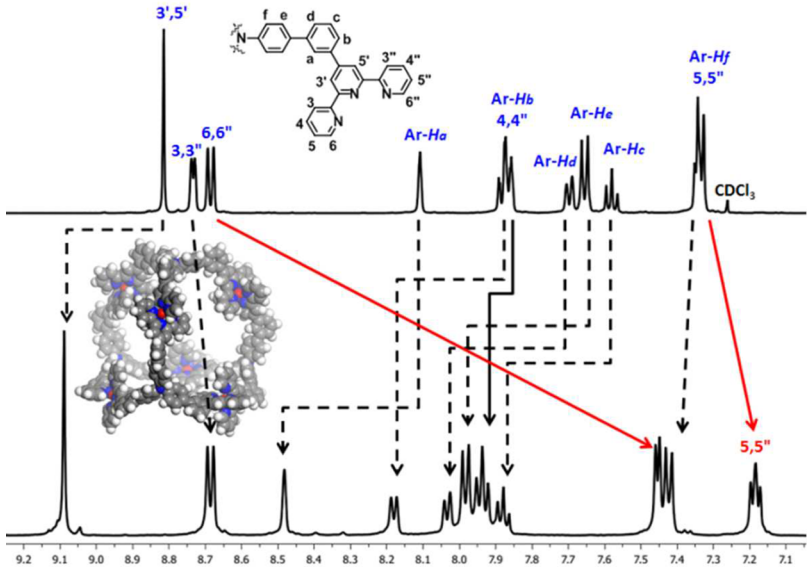

Figure 1. Stacked ^{1}H NMR spectra of tris-terpyridine **3** (above) and nanosphere **4** (below). Arrows depict assigned resonance shifts that occur upon complex formation.

Ru^{2+}.[37] In order to understand the effect of introducing flexibility into the assembly process, a new tris-terpyridine linker **3** was synthesized using a triphenylamine core. The single step, kinetically controlled assembly of **3** with Ru^{2+} leads to the formation of a terpyridine-based, highly symmetric, 3D-nanocage **4**. To demonstrate the potential of employing different modes of <tpy-M^{2+}-tpy> connectivity to control the shape and size of the resulting supramolecular architecture, linker **3** was reacted with Ru^{2+} to form a key monoRu^{2+} dimer **5** intermediate. Complexation between dimer **5** with Fe^{2+} exhibits the unexpected temperature-dependent formation of two unique isomeric 3D nanoarchitectures **6a** and **6b**. Moreover, the treatment of **5** with Ru^{2+} results in the formation of a new, ruthenium, 3D molecular complex **7**, which is structurally similar to that of complex **6a**, rather than producing nanosphere **4**. Structural confirmation was accomplished using ESI-TWIM mass spectrometry, 1D and 2D NMR, ^{1}H DOSY NMR, and TEM imaging methods. Additionally, the structure of nanosphere **4** was definitively characterized by single crystal X-ray crystallography.

RESULTS AND DISCUSSION

Initially, a three-fold, Suzuki cross-coupling[54] reaction between tris(4-bromophenyl)amine (**1**)[55] and boronic acid **2** (prepared from 3-formylphenylboronic acid with 2-acetylpyridine and base, followed by NH_4OAc)[37] subsequently gave (70%) the desired tris-dentate **3** (Scheme 1). The ^{1}H NMR spectrum of **3** exhibited one set of signals attributed to both terpyridine moieties and aryl groups supporting its overall three-fold symmetry.

Treatment of **3** with $Ru(DMSO)_4Cl_2$ in a 2:3 ratio in a $CHCl_3$ and MeOH mixture (2:1, v/v) under reflux for 24 h

DOI: 10.1021/jacs.6b11784
J. Am. Chem. Soc. 2017, 139, 3012−3020

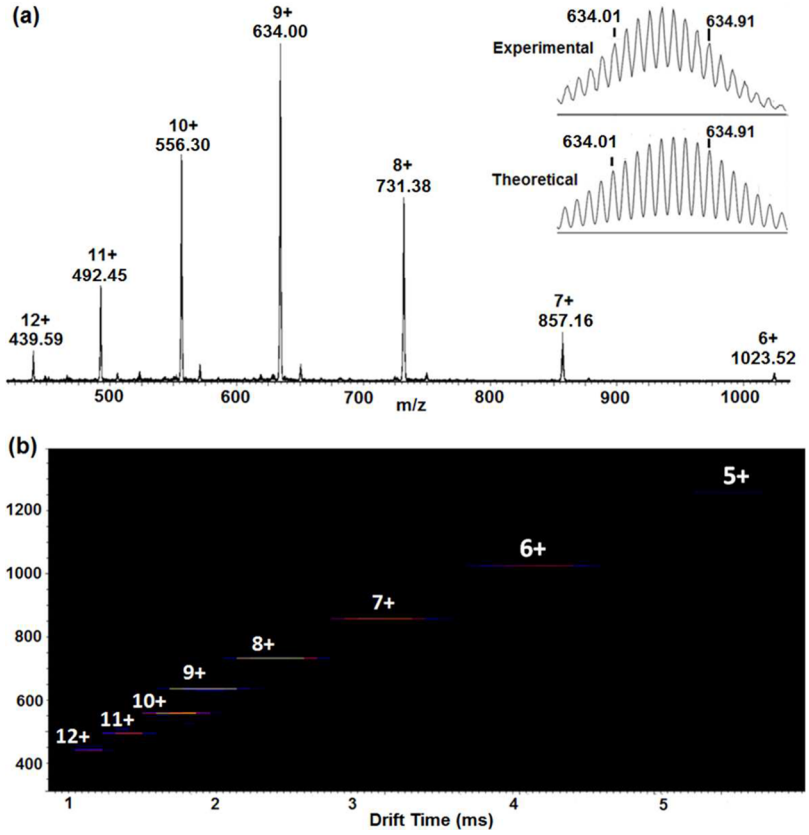

Figure 2. (a) ESI-MS and (b) 2D ESI-TWIM-MS plot (m/z vs drift time) for **4**. The charge states of the intact assemblies are marked.

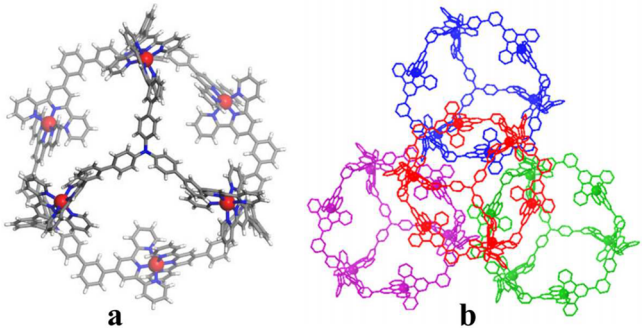

Figure 3. (a) Single crystal structure of nanosphere **4**. (b) The packing of four molecules of **4** showing ball-like stacking. The counterions and solvent molecules were highly disordered; thus, these groups along with all of the disordered pyridinyl rings have not been included in the structural model that is based on X-ray diffraction.

resulted in the formation of a translucent deep red solution. After concentration and column chromatography (SiO_2) with H_2O-MeCN-saturated KNO_3 (1:20:1; v/v/v), the desired complex **4** was isolated (32%), as its nitrate salt. Subsequent treatment with excess aqueous NH_4PF_6 solution gave **4** with PF_6^- counterions. The ^{1}H NMR spectrum of **4** (CD_3CN, 300 K) exhibited one set of sharp well-resolved peaks indicative of the formation of a single, highly symmetric discrete architecture. The assignment of terpyridine and aromatic protons was readily achieved based on 2D COSY and 2D NOESY NMR analysis. The 6,6″ doublet of the terpyridine unit was significantly shifted upfield to 7.45 ppm due to the shielding effect of opposing perpendicular ring currents, as is characteristic of pseudo-octahedral <tpy-Ru^{2+}-tpy> connectivity (Figure 1). Further, the expected downfield shift of the tpy$H^{3',5'}$ singlet from 8.85 to 9.09 ppm also supports metal–ligand complex formation (Figure 1).

The structure of nanosphere **4** was confirmed by its ESI-MS spectrum, showing a series of dominant peaks at m/z 1023.52, 857.16, 731.38, 634.01, 556.30, and 492.45 amu corresponding to ions with charge states 6+ to 11+ (Figure 2a), thereby supporting the assembly of 4 ligands, 6 metals, and 12 PF_6^- anions. The ESI-TWIM-MS, in which ion m/z values are plotted against ion drift time,[56−58] further validates the structural conformation of **4** by exhibiting a single band with narrow drift time distribution for each charge state with expected step patterns (Figure 2b), indicating the presence of a single structural conformer or isomer ruling out the possibility of other components.

The structure of complex **4** was further confirmed by collisional cross-section (CCS) analysis of ions deduced from their drift times measured by TWIM-MS experiment. The experimental CCSs for charge states 8−11 were found to be 942.35, 968.40, 1000.44, and 1031.09 Å^2, respectively. The nominal CCSs differences between these charge states (balanced by 4, 3, 2, and 1 PF_6^- counterions, respectively) suggest that **4** possesses a very rigid, shape-persistent geometry. The average experimental CCSs of all charge states (985.57 ± 04 Å^2) corroborates well with theoretically predicted CCSs of the counterion-free complex (984.06 ± 03 Å^2), which was calculated from 100 energy-minimized structures using the trajectory method,[59−61] further supporting the proposed architecture. The ^{1}H 2D DOSY NMR spectrum of **4** (Figure S11) clearly shows a single diffusion band indicative of a single species in CD_3CN and rules out the possibility of any other macrocyclic or oligomeric products.

DOI: 10.1021/jacs.6b11784
J. Am. Chem. Soc. 2017, 139, 3012−3020

Scheme 2. Temperature-Dependent Synthesis of Complexes 6a and 6b from monoRu^{2+} Terpyridinyl Dimer 5

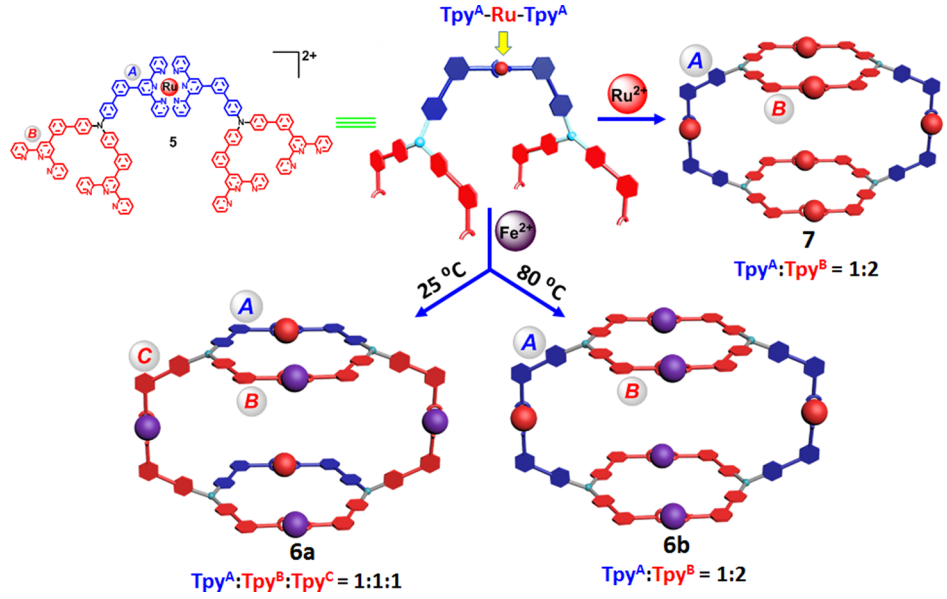

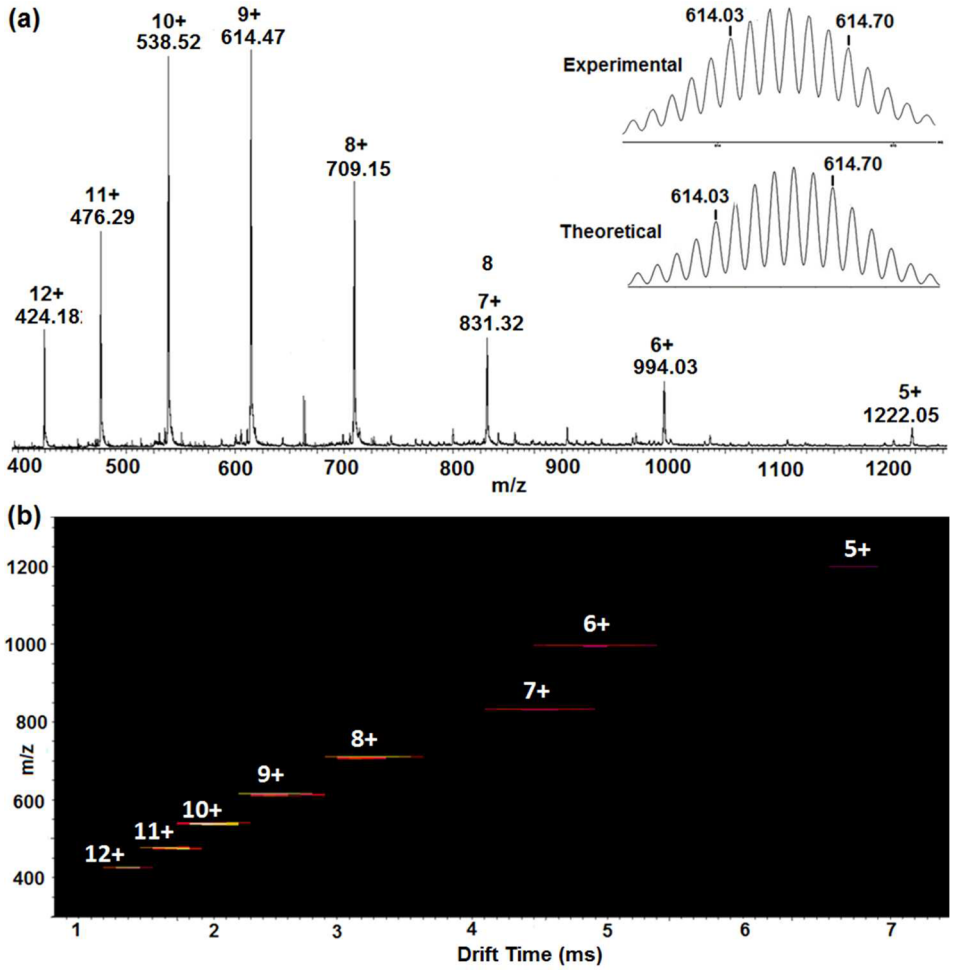

Figure 4. (a) ESI-MS and (b) 2D ESI-TWIM-MS plot (m/z vs drift time) for **6a**. The charge states of the intact assemblies are marked.

Following the MS and NMR characterization, the structure of nanosphere **4** was unequivocally confirmed by single crystal X-ray diffraction analysis (Figure 3). A red single crystal was obtained by vapor diffusion of EtOAc into a DMF solution of **4** over a period of 2 weeks. Owing to the large volume of the spherical complex, the presence of disordered flexible ligand, solvent molecules, and numerous counterions, the diffraction spots were observed only up to resolution of ca. 1.7 Å.

DOI: 10.1021/jacs.6b11784
J. Am. Chem. Soc. 2017, 139, 3012−3020

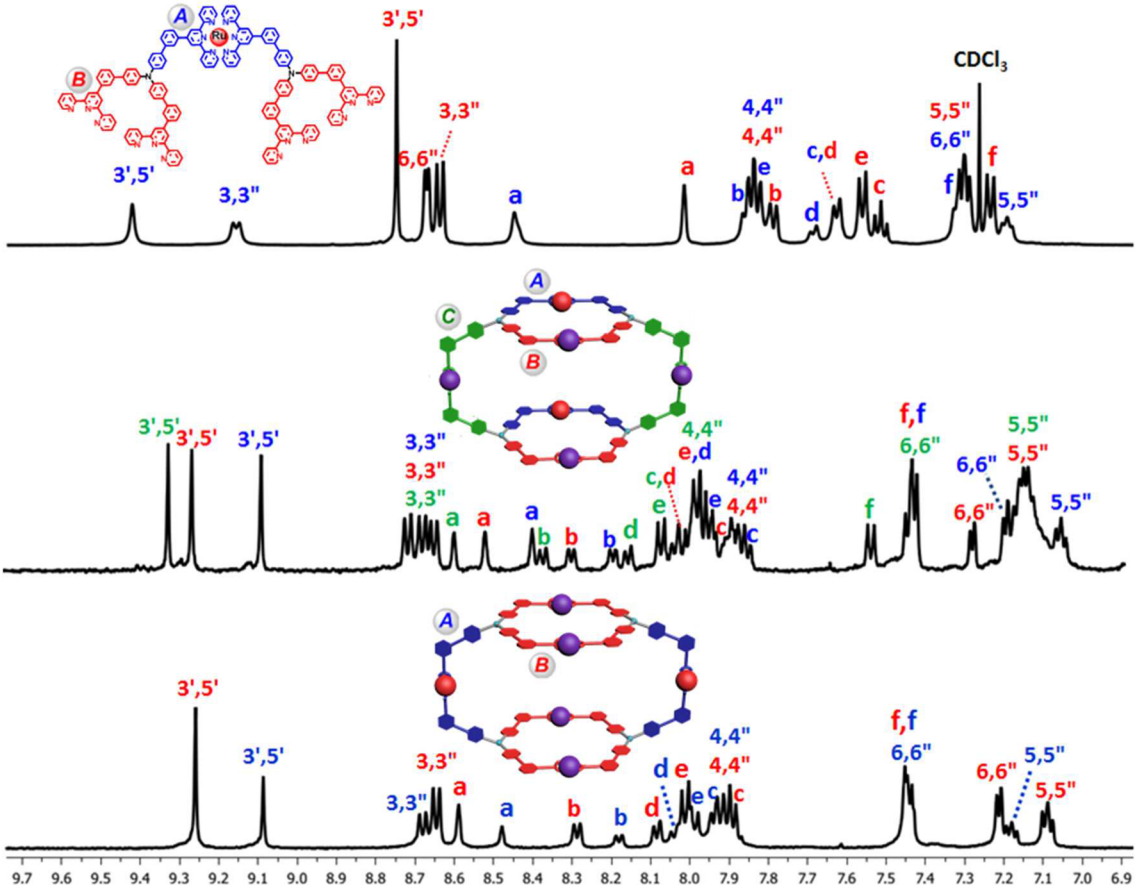

Figure 5. Stacked ^{1}H NMR spectra of monoRu^{2+} dimer **5** (above), complex **6a** (middle), and complex **6b** (below). The numbering of the signals for the three nonequivalent terpyridine units of arm *A*, *B*, and *C* of complex **6a** are represented in red, blue, and green colors for better representation of ^{1}H NMR spectral data.

However, despite the low resolution, heavy disorder, and relatively high R-factor, it was sufficient to model the relative position of four ligands and six Ru^{2+} ions, thereby establishing the basic connectivity of the metal organic polyhedron **4**, which is consistent with the computer generated model. As expected a highly symmetric, shape-persistent molecular cage was revealed and shown to pack into a trigonal crystal possessing the $R\bar{3}$ space group. These cage molecules pack together in a unique arrangement in which three adjacent 3D molecules penetrate into the vacant inner space of one cage via a noninterlocking fashion, thus allowing $\pi-\pi$ interactions between the ligand backbones. The six ruthenium atoms adopt a slightly distorted octahedral geometry, where the longest distance between two nearby Ru^{2+} atoms is 20.6 Å, the average distance across the interior is ca. 27 Å, and an overall volume is 4603 Å^3.

Inspired by the formation of this octahedral nanosphere, we wanted to study the effect of rigidity on this coordination bonding approach of the tris-terpyridine linker as well as on the shape and size of resulting macromolecular complex. Thus, we preblocked one tpy arm of tris-dentate **3** by dimerization, which resulted in two identical tpy units from two tris-ligands being connected through a rigid <tpy-Ru^{2+}-tpy> linkage. The monoRu^{2+} terpyridinyl dimer **5** was synthesized by a stoichiometrically controlled reaction of **3** with Ru(DMSO)$_4$Cl$_2$ in a mixture of CHCl$_3$/MeOH (1:1, v/v) for 24 h. After column chromatography, the desired dimer **5** (2Cl$^-$) was obtained in 35% yield. A consistent ESI-MS signal at m/z = 1217.87 for [**5**-2Cl]$^{2+}$ was obtained, and its ^{1}H NMR spectrum also confirmed the formation of desired dimer **5**, with the appearance of two singlets at 9.42 and 8.75 ppm in a 1:2 peak ratio expected for two different sets of 3′,5′ protons from the coordinated and noncoordinated terpyridines, respectively (Supporting Information). All other NMR peaks were assigned with the aid of 2D COSY and NOESY NMR analysis.

To study how the introduction of rigidity by preblocking one coordination site via a single stable <tpy-Ru^{2+}-tpy> bond affects the coordination behavior of tris-dentate ligand, dimer **5** was treated with FeCl$_2$ in 1:2 ratio in CHCl$_3$/MeOH (1:1, v/v) for 24 h at 25 °C generating a translucent purple solution (Scheme 2). After purification over silica with H$_2$O-MeCN-saturated KNO$_3$ (aq) (1:20:1; v/v/v), **6a** (12NO$_3^-$) was obtained (25%). The counterions were exchanged using excess aqueous NH$_4$PF$_6$ to give complex **6a**, which was characterized by ESI-MS and NMR experiments.

The ESI-MS spectrum of **6a** revealed a series of intense peaks with charge states 5+ to 12+ via the consecutive loss of the PF$_6^-$ counterions (Figure 4a). Based on the mass to charge ratio of these ions, **6a** is composed of precisely two dimers (**5**), four Fe^{2+} ions, and 12 PF$_6^-$ counterions. These peaks were isotopically resolved and found to be in agreement with the corresponding simulated isotopic distribution. Additional evidence supporting the structural composition of **6a** was provided by ESI-TWIM-MS, which exhibited a single band with a narrow drift time distribution for charge states 5+ to 12+, suggesting the presence of a single structure (Figure 4b).

DOI: 10.1021/jacs.6b11784
J. Am. Chem. Soc. 2017, 139, 3012−3020

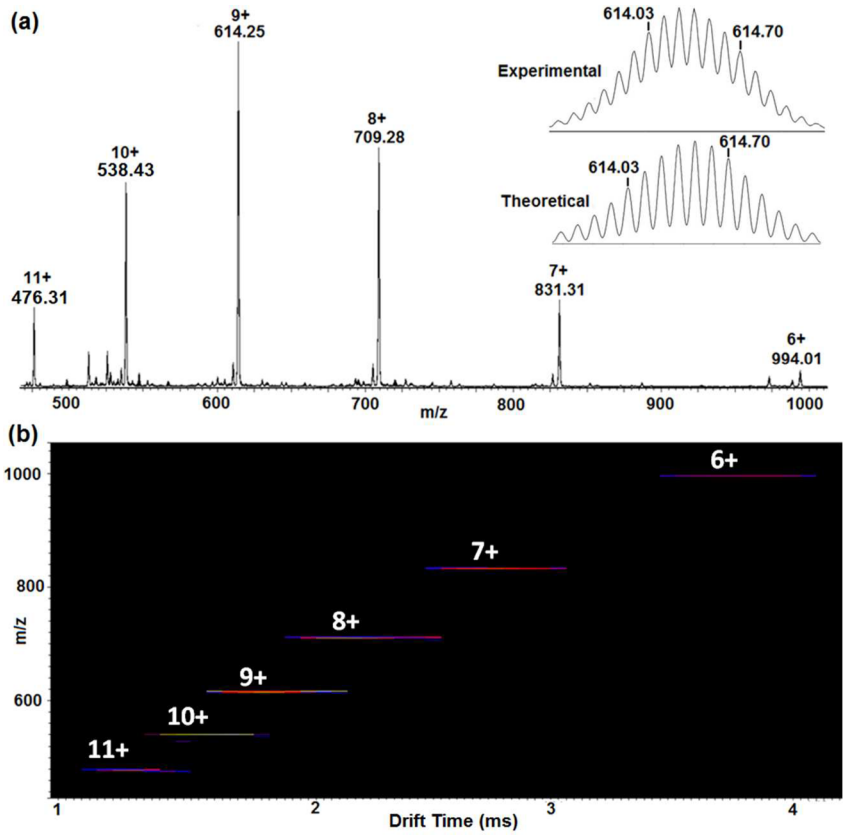

Figure 6. (a) ESI-MS and (b) 2D ESI-TWIM-MS plot (m/z vs drift time) for **6b**. The charge states of the intact assemblies are marked.

Table 1. Drift Times and Collision Cross Sections for Complexes 6a and 6b

charge state [+]	drift time [ms]	collision cross sections [Å^2]		
		expt	expt average	calcd average
Complex **6a**				
5	5.01	855.47		
6	3.84	924.34		
7	3.62	1054.30		
8	2.63	1062.44	1026.72 ± 03	982.05 ± 02
9	2.06	1085.52		
10	1.67	1110.27		
11	1.23	1094.70		
Complex **6b**				
5	5.69	898.51		
6	4.15	952.17		
7	3.79	1072.15		
8	2.89	1101.00	1062.06 ± 02	983.26 ± 02
9	2.23	1117.91		
10	1.81	1143.72		
11	1.44	1148.92		

Complex **6a** was also characterized by ^{1}H NMR spectroscopy, which revealed three different tpy units in a 1:1:1 integration ratio (Figure 5), which suggests a novel 3D geometry for cage **6a**, where one <tpy-Fe^{2+}-tpy> side is parallel with <tpy-Ru^{2+}-tpy> forming two rims; whereas, the other perpendicular <tpy-Fe^{2+}-tpy> connects both rims. Assignment of all NMR peaks was achieved based on 2D COSY and NOESY NMR spectroscopy. Three distinct singlets at 9.30, 9.24, and 9.06 ppm exhibit a precise peak ratio (1:1:1) for the three different 3′,5′-protons of arms *A*, *B*, and *C*, respectively. The noteworthy features of this spectra include the observation that all 6,6″ protons are shifted significantly upfield as a result of shielding effects, suggesting complete metal−ligand complexation by each tpy unit, which further validates the structure of **6a**.

Following unambiguous structural confirmation of complex **6a** by NMR and MS analysis, a temperature-dependent phenomenon directed us to get some insight into its formation. When dimer **5** was treated with $FeCl_2$ in similar manner but at a higher temperature (65 °C), the resultant reaction mixture was found to contain a new band along with that of complex **6a** on a silica gel TLC plate having an R_f value (0.3; H_2O-MeCN-saturated aq KNO_3; 1:20:1; v/v/v) that was less than that of complex **6a** (R_f = 0.4). After chromatography and subsequent exchange of the counterions to PF_6^-, the new complex **6b** was obtained as a purple solid. After further increasing the reaction temperature to 80 °C, the TLC band for **6a** completely disappeared, and only the complex **6b** was obtained.

The ESI-MS spectrum of **6b** exhibited a series of peaks for the charge states identical to that of **6a** (Figure 6a). Also, the TWIM-MS spectrum suggests the presence of a solitary species due to the appearance of a single band with narrow charge distribution for each charge state (Figure 6b), thus confirming the identical chemical composition for both **6a** and **6b**. But, unlike complex **6a**, the ^{1}H NMR spectrum of **6b** revealed two sets of 3′,5′-tpy protons in a 2:1 ratio (Figure 5). The observed NMR and mass spectral data suggest that **6b** is a structural isomer of **6a**, where perpendicular <tpy-Fe^{2+}-tpy> connectivity switched positions with the <tpy-Ru^{2+}-tpy> unit to adopt a more symmetrical 3D conformation. The overall structure of **6b** is similar to that of **6a** except now both of the <tpy-Fe^{2+}-

DOI: 10.1021/jacs.6b11784
J. Am. Chem. Soc. 2017, 139, 3012−3020

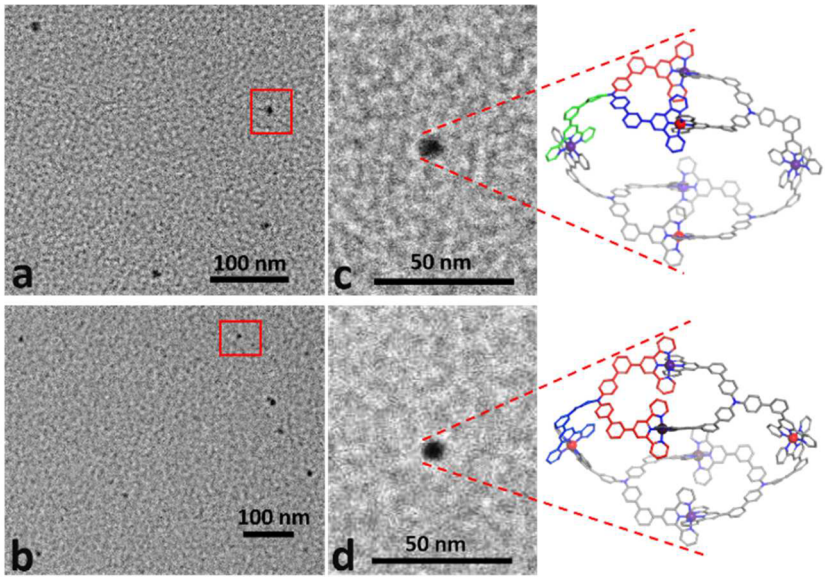

Figure 7. TEM images of **6a** (a) and **6b** (b) obtained on a carbon-coated Cu grid. The high-magnification TEM images (c and d) clearly exhibit oval-shaped rounded pictures of the proposed computer-generated, energy-minimized structure of **6a** and **6b**, respectively.

tpy> sides are parallel; the appearance of two tpy$^{3',5'}$ singlets at 9.26 and 9.08 ppm are for arms *A* and *B*, respectively. The tpy$H^{6,6''}$ doublet noticeably shifted upfield when compared with the dimer **5**. All of the peaks in ^{1}H NMR were assigned and verified with the aid of 2D COSY and 2D NOESY experiments; they are in complete agreement with the proposed structure. In diffusion ordered NMR spectroscopy (DOSY), all signals exhibit a single narrow band for both complexes **6a** and **6b** (Figure S27, Supporting Information), affirming that they are very similar in size, consistent with the common connectivity in both complexes. Additionally, the appearance of a single diffusion trace further confirmed the presence of a single species in solution.

To further confirm the connectivity pattern in complex **6b**, Ru^{2+} dimer **5** was treated with $Ru(DMSO)_4Cl_2$ in $CHCl_3$/MeOH under identical conditions (Scheme 2). Thus, if the ligand connectivity pattern based on NMR and MS is correct for complex **6b**, the use of Ru^{2+} would give rise to a structurally similar ruthenium cage **7** with nearly identical connectivity pattern. After being purified over silica gel, complex **7** was obtained in moderate to good yield. The ESI-MS spectrum of **7** exhibited a series of peaks identical to those obtained for **4** (Supporting Information). The isotopic distribution of each charge state was found to be in agreement with the simulated isotope pattern. The ESI-TWIM-MS suggests the presence of a single isomer by exhibiting charge states with narrow drift time distributions, which further confirmed the identical structural composition for complexes **7** and **4**. But unlike **4**, the ^{1}H NMR spectrum of **7** revealed two sets of terpyridine units with 2:1 integration ratio and upfield shifted 6,6″ protons for all tpy units, thereby supporting the presence of no uncomplexed tpy moieties. All NMR peaks were assigned based on detailed analyses of 2D COSY and NOESY spectra (Supporting Information). The presence of two chemically nonequivalent <tpy-Ru^{2+}-tpy> connectivities in 2:1 ratio clearly confirmed that complex **7** adopts a structure similar to that of complex **6b**. These results further validate the predicted structural conformation for both **6a** and **6b**.

CCSs of several charge states for both **6a** and **6b** were determined from the drift times measured in TWIM-MS experiments. The CCS can be considered as the average forward moving surface area of ions, thereby representing the size of corresponding ion as well as architecture. The CCSs varied slightly with charge state for **6a** and **6b**, suggesting structural rigidity. The average experimental CCSs for cages **6a** and **6b** were very similar, signifying that these two assemblies possess kindred configurations. The theoretical CCSs were also calculated on the basis of 100 energy-minimized structures for each complex using the trajectory (TJ) method. The average theoretical CCSs of cages **6a** and **6b** correlate well with the corresponding average experimental CCSs supporting the proposed architectures (Table 1). The CCSs simulated by TJ model and the corresponding experimental CCSs differ by <5% for **6a** and 8% for **6b**.

Transmission electron microscopy (TEM) experiments were performed to visualize the geometry of the 3D complexes **6a** and **6b** (Figure 7). The TEM images revealed a direct correlation of both shape and size of individual molecules upon deposition of dilute MeCN solution (ca. 10^{-6} M) of complexes **6a** and **6b** on carbon-coated grids (Cu, 400 mesh). The structural frameworks showed an outline of a uniform dispersion of individual molecules with clear edges (Figure 7). The observed dimensions of discrete nanostructures for both **6a** and **6b** were corroborated with molecular modeling. The average distance between the furthest edges, 4.9 and 4.7 nm for **6a** and **6b**, respectively, correlates well with the size obtained from optimized molecular models.

■ CONCLUSIONS

We have designed and synthesized a terpyridine-based nanosphere by the combination of four flexible tris-terpyridine linkers with six Ru^{2+} ions in one-step. Along with conventional characterization by NMR spectroscopy and ESI-MS analysis, the nanosphere's structure was unequivocally determined by single crystal X-ray crystallography. In order to study the effects of structural rigidity in the coordination process, the corresponding dimer of tris-dentate ligand was synthesized via employing <tpy-Ru^{2+}-tpy> connectivity. The complexation of this Ru^{2+}-dimer with Fe^{2+} at ambient temperature gave a

DOI: 10.1021/jacs.6b11784
J. Am. Chem. Soc. 2017, 139, 3012−3020

mixture of two isomeric nanocages; whereas at elevated temperatures, the more thermodynamically stable 3D product was exclusively generated. This phenomenon offers a new insight for the construction of stable complex 3D metallosupramolecular architectures, demonstrating the potential to employ different metals in <tpy-M^{2+}-tpy> connectivity can give access to different stable isomeric nanoconstructs.

■ ASSOCIATED CONTENT

Supporting Information

The Supporting Information is available free of charge on the ACS Publications website at DOI: 10.1021/jacs.6b11784.

Details of the synthesis, spectroscopic data, and computation details for **1**–**7** (PDF)

Crystal data and structure refinement for **4** (CIF)

■ AUTHOR INFORMATION

Corresponding Authors

*wesdemiotis@uakron.edu

*newkome@uakron.edu

ORCID

Sourav Chakraborty: 0000-0001-5564-3087

Wei Hong: 0000-0001-7866-9917

Chrys Wesdemiotis: 0000-0002-7916-4782

George R. Newkome: 0000-0001-6019-5071

Author Contributions

⊥These authors contributed equally.

Notes

The authors declare no competing financial interest.

■ ACKNOWLEDGMENTS

We gratefully thank the National Science Foundation (CHE-1151991 to G.R.N. and CHE-1308307 to C.W.) for financial support and Jessi A. Baughman (UA) for valuable expertise and assistance with the DOSY NMR experiment.

■ REFERENCES

(1) Bates, A. D.; Maxwell, A. *DNA Topology*; Oxford University Press: New York, 2005.

(2) Buxbaum, E. *Fundamentals of Protein Structure & Function*; Springer Science + Business Media: LLC: New York, 2007.

(3) Iinuma, R.; Ke, Y.; Jungmann, R.; Schlichthaerle, T.; Woehrstein, J. B.; Yin, P. *Science* **2014**, *344*, 65−69.

(4) Cook, T. R.; Stang, P. J. *Chem. Rev.* **2015**, *115*, 7001−7045.

(5) Saha, M. L.; Neogi, S.; Schmittel, M. *Dalton Trans.* **2014**, *43*, 3815−3834.

(6) Sun, Q. F.; Iwasa, J.; Ogawa, D.; Ishido, Y.; Sato, S.; Ozeki, T.; Sei, Y.; Yamaguchi, K.; Fujita, M. *Science* **2010**, *328*, 1144−1147.

(7) Newkome, G. R.; Moorefield, C. N. *Chem. Soc. Rev.* **2015**, *44*, 3954−3967.

(8) Clegg, J. K.; Li, F.; Lindoy, L. F. *Coord. Chem. Rev.* **2013**, *257*, 2536−2550.

(9) Mukherjee, S.; Mukherjee, P. S. *Chem. Commun.* **2014**, *50*, 2239−2248.

(10) Sato, S.; Murase, T.; Fujita, M. Self-Assembly of Coordination Cages and Spheres. In *Supramolecular Chemistry*; John Wiley & Sons, Ltd: Chichester, U.K., 2012.

(11) Smulders, M. M. J.; Riddell, I. A.; Browne, C.; Nitschke, J. R. *Chem. Soc. Rev.* **2013**, *42*, 1728−1754.

(12) Chakrabarty, R.; Mukherjee, P. S.; Stang, P. J. *Chem. Rev.* **2011**, *111*, 6810−6918.

(13) Cook, T. R.; Zheng, Y.-R.; Stang, P. J. *Chem. Rev.* **2013**, *113*, 734−777.

(14) Carnes, M. E.; Collins, M. S.; Johnson, D. W. *Chem. Soc. Rev.* **2014**, *43*, 1825−1834.

(15) Fujita, D.; Ueda, Y.; Sato, S.; Yokoyama, H.; Mizuno, N.; Kumasaka, T.; Fujita, M. *Chem.* **2016**, *1*, 91−101.

(16) Han, M.; Engelhard, D. M.; Clever, G. H. *Chem. Soc. Rev.* **2014**, *43*, 1848−1860.

(17) Chakraborty, S.; Mondal, S.; Bhowmick, S.; Ma, J.; Tan, H.; Neogi, S.; Das, N. *Dalton Trans.* **2014**, *43*, 13270−13277.

(18) Lippert, B.; Sanz Miguel, P. J. *Chem. Soc. Rev.* **2011**, *40*, 4475−4487.

(19) Wang, W.; Wang, Y. X.; Yang, H. B. *Chem. Soc. Rev.* **2016**, *45*, 2656−2693.

(20) Caulder, D. L.; Brückner, C.; Powers, R. E.; König, S.; Parac, T. N.; Leary, J. A.; Raymond, K. N. *J. Am. Chem. Soc.* **2001**, *123*, 8923−8938.

(21) Frank, M.; Johnstone, M. D.; Clever, G. H. *Chem. - Eur. J.* **2016**, *22*, 14104−14125.

(22) McConnell, A. J.; Wood, C. S.; Neelakandan, P. P.; Nitschke, J. R. *Chem. Rev.* **2015**, *115*, 7729−7793.

(23) Yan, X.; Xu, D.; Chi, X.; Chen, J.; Dong, S.; Ding, X.; Yu, Y.; Huang, F. *Adv. Mater.* **2012**, *24*, 362−369.

(24) Wang, F.; Zhang, J.; Ding, X.; Dong, S.; Liu, M.; Zheng, B.; Li, S.; Wu, L.; Yu, Y.; Gibson, H. W.; Huang, F. *Angew. Chem., Int. Ed.* **2010**, *49*, 1090−1094.

(25) Schubert, U. S.; Hofmeier, H.; Newkome, G. R. *Modern Terpyridine Chemistry*; Wiley-VCH: Weinheim, 2006.

(26) Ludlow, J. M., III; Newkome, G. R. Progress in Heterocyclic Metallosupramolecular Construction. In *Advances in Heterocyclic Chemistry*; Academic Press: Cambridge, MA, 2016; pp 195−236.

(27) Wang, S. Y.; Fu, J. H.; Liang, Y. P.; He, Y. J.; Chen, Y. S.; Chan, Y. T. *J. Am. Chem. Soc.* **2016**, *138*, 3651−3654.

(28) Li, Y.; Jiang, Z.; Wang, M.; Yuan, J.; Liu, D.; Yang, X.; Chen, M.; Yan, J.; Li, X.; Wang, P. *J. Am. Chem. Soc.* **2016**, *138*, 10041−10046.

(29) Wang, M.; Wang, K.; Wang, C.; Huang, M.; Hao, X. Q.; Shen, M. Z.; Shi, G. Q.; Zhang, Z.; Song, B.; Cisneros, A.; Song, M. P.; Xu, B.; Li, X. *J. Am. Chem. Soc.* **2016**, *138*, 9258−9268.

(30) Schultz, A.; Cao, Y.; Huang, M.; Cheng, S. Z. D.; Li, X.; Moorefield, C. N.; Wesdemiotis, C.; Newkome, G. R. *Dalton Trans.* **2012**, *41*, 11573−11575.

(31) Newkome, G. R.; Cho, T. J.; Moorefield, C. N.; Baker, G. R.; Saunders, M. J.; Cush, R.; Russo, P. S. *Angew. Chem., Int. Ed.* **1999**, *38*, 3717−3721.

(32) Wang, J.-L.; Li, X.; Lu, X.; Hsieh, I.-F.; Cao, Y.; Moorefield, C. N.; Wesdemiotis, C.; Cheng, S. Z. D.; Newkome, G. R. *J. Am. Chem. Soc.* **2011**, *133*, 11450−11453.

(33) Lu, X.; Li, X.; Cao, Y.; Schultz, A.; Wang, J.-L.; Moorefield, C. N.; Wesdemiotis, C.; Cheng, S. Z. D.; Newkome, G. R. *Angew. Chem., Int. Ed.* **2013**, *52*, 7728−7731.

(34) Newkome, G. R.; Wang, P.; Moorefield, C. N.; Cho, T. J.; Mohapatra, P.; Li, S.; Hwang, S.-H.; Lukoyanova, O.; Echegoyen, L.; Palagallo, J. A.; Iancu, V.; Hla, S.-W. *Science* **2006**, *312*, 1782−1785.

(35) Sarkar, R.; Guo, K.; Moorefield, C. N.; Saunders, M. J.; Wesdemiotis, C.; Newkome, G. R. *Angew. Chem., Int. Ed.* **2014**, *53*, 12182−12185.

(36) Chakraborty, S.; Sarkar, R.; Endres, K.; Xie, T. Z.; Ghosh, M.; Moorefield, C. N.; Saunders, M. J.; Wesdemiotis, C.; Newkome, G. R. *Eur. J. Org. Chem.* **2016**, *2016*, 5091−5095.

(37) Xie, T.-Z.; Liao, S.-Y.; Guo, K.; Lu, X.; Dong, X.; Huang, M.; Moorefield, C. N.; Cheng, S. Z. D.; Liu, X.; Wesdemiotis, C.; Newkome, G. R. *J. Am. Chem. Soc.* **2014**, *136*, 8165−8168.

(38) Xie, T.-Z.; Guo, K.; Guo, Z.; Gao, W.-Y.; Wojtas, L.; Ning, G.-H.; Huang, M.; Lu, X.; Li, J.-Y.; Liao, S.-Y.; Chen, Y.-S.; Moorefield, C. N.; Saunders, M. J.; Cheng, S. Z. D.; Wesdemiotis, C.; Newkome, G. R. *Angew. Chem., Int. Ed.* **2015**, *54*, 9224−9229.

(39) Xie, T. Z.; Endres, K. J.; Guo, Z.; Ludlow, J. M., III; Moorefield, C. N.; Saunders, M. J.; Wesdemiotis, C.; Newkome, G. R. *J. Am. Chem. Soc.* **2016**, *138*, 12344−12347.

(40) Xie, T.-Z.; Guo, K.; Huang, M.; Lu, X.; Liao, S.-Y.; Sarkar, R.; Moorefield, C. N.; Cheng, S. Z. D.; Wesdemiotis, C.; Newkome, G. R. *Chem. - Eur. J.* **2014**, *20*, 11291−11294.
(41) Lu, X.; Li, X.; Guo, K.; Xie, T.-Z.; Moorefield, C. N.; Wesdemiotis, C.; Newkome, G. R. *J. Am. Chem. Soc.* **2014**, *136*, 18149−18155.
(42) Schmittel, M.; He, B. *Chem. Commun.* **2008**, 4723−4725.
(43) Schmittel, M.; He, B.; Mal, P. *Org. Lett.* **2008**, *10*, 2513−2516.
(44) Wang, Y. C.; Liang, Y. P.; Cai, J. Y.; He, Y. J.; Lee, Y. H.; Chan, Y. T. *Chem. Commun.* **2016**, *52*, 12622−12625.
(45) Schroder, T.; Brodbeck, R.; Letzel, M. C.; Mix, A.; Schnatwinkel, B.; Tonigold, M.; Volkmer, D.; Mattay, J. *Tetrahedron Lett.* **2008**, *49*, 5939−5942.
(46) Winter, A.; Gottschaldt, M.; Newkome, G. R.; Schubert, U. S. *Curr. Top. Med. Chem.* **2012**, *12*, 158−175.
(47) Schubert, U. S.; Winter, A.; Newkome, G. R. *Terpyridine-based Materials-For Catalytic, Optoelectronic, and Life Science Applications*; Wiley-VCH: Weinheim, 2011.
(48) Siebert, R.; Winter, A.; Schmitt, M.; Popp, J. Ã.; Schubert, U. S.; Dietzek, B. *Macromol. Rapid Commun.* **2012**, *33*, 481−497.
(49) Yam, V. W.-W.; Au, V. K.-M.; Leung, S. Y.-L. *Chem. Rev.* **2015**, *115*, 7589−7728.
(50) Winter, A.; Hoeppener, S.; Newkome, G. R.; Schubert, U. S. *Adv. Mater.* **2011**, *23*, 3484−3498.
(51) Ludlow, J. M., III; Guo, Z.; Schultz, A.; Sarkar, R.; Moorefield, C. N.; Wesdemiotis, C.; Newkome, G. R. *Eur. J. Inorg. Chem.* **2015**, *2015*, 5662−5668.
(52) Li, Y.; Jiang, Z.; Yuan, J.; Wu, T.; Moorefield, C. N.; Newkome, G. R.; Wang, P. *Chem. Commun.* **2015**, *51*, 5766−5769.
(53) Schultz, A.; Li, X.; Barkakaty, B.; Moorefield, C. N.; Wesdemiotis, C.; Newkome, G. R. *J. Am. Chem. Soc.* **2012**, *134*, 7672−7675.
(54) Miyaura, N.; Yanagi, T.; Suzuki, A. *Synth. Commun.* **1981**, *11*, 513−519.
(55) Shi, D.; Ren, Y.; Jiang, H.; Cai, B.; Lu, J. *Inorg. Chem.* **2012**, *51*, 6498−6506.
(56) Hilton, G. R.; Jackson, A. T.; Thalassinos, K.; Scrivens, J. H. *Anal. Chem.* **2008**, *80*, 9720−9725.
(57) Hoaglund-Hyzer, C. S.; Counterman, A. E.; Clemmer, D. E. *Chem. Rev.* **1999**, *99*, 3037−3079.
(58) Li, X.; Chan, Y.-T.; Newkome, G. R.; Wesdemiotis, C. *Anal. Chem.* **2011**, *83*, 1284−1290.
(59) Clemmer, D. E.; Jarrold, M. F. *J. Mass Spectrom.* **1997**, *32*, 577−592.
(60) Jarrold, M. F. *Annu. Rev. Phys. Chem.* **2000**, *51*, 179.
(61) Shvartsburg, A. A.; Liu, B.; Siu, K. W. M.; Ho, K. M. *J. Phys. Chem. A* **2000**, *104*, 6152−6157.

DOI: 10.1021/jacs.6b11784
J. Am. Chem. Soc. 2017, 139, 3012−3020